Point Defects and Alloy Incorporation in Ultrawide Bandgap β-(Al$_x$Ga$_{1-x}$)$_2$O$_3$ Films

Hsien-Lien Huang[1], Jared Johnson[1], Chris Chae[1], A F M Anhar Uddin Bhuiyan[2], Zixuan Feng[2], Nidhin Kurian Kalarickal[2], Siddharth Rajan[2], Hongping Zhao[2] and Jinwoo Hwang[1]

[1]Materials Science and Engineering, The Ohio State University, United States, [2]Electrical and Computer Engineering, The Ohio State University, United States

The development of novel ultrawide band gap (UWBG) semiconductors requires a precise understanding of the point defects and their complexes that govern the materials' electronic and photonic properties. β-Ga$_2$O$_3$ has gained recent attention as a viable candidate for power device applications due to its large band gap (4.8 eV) and high breakdown voltage [1]. Recently, we have reported that the defect trap states in β-Ga$_2$O$_3$ is closely related to the unique formation of point defects and their complexes [2]. Based on this finding, we have extended our study to investigate the growth characteristics and electronic properties of β-(Al$_x$Ga$_{1-x}$)$_2$O$_3$. The main benefits of β-(Al$_x$Ga$_{1-x}$)$_2$O$_3$ include the high channel mobility at the interface, as well as being able to achieve a tunable band gap, which may overcome some of the barriers existing in the fabrication of β-Ga$_2$O$_3$ based devices. Despite the promises, the growth and application of β-(Al$_x$Ga$_{1-x}$)$_2$O$_3$ films and heterostructures still remain at a nascent stage. Our goal in this study is to (*i*) identify the dominant mechanism of the Al atom incorporation into β-Ga$_2$O$_3$ when alloying, and (*ii*) determine the detailed structure of point and extended defects in these films that affect the growth characteristics and important properties of the heterostructure devices.

Our approach is based on the quantitative analysis of the atomic column intensities in scanning transmission electron microscopy (STEM) images that reveal the details of the atomic arrangement within each column, providing the information about how many point defects, including interstitials, substitutional, as well as cation vacancies, are present within the material (Fig. 1) [3]. Explicit quantification of the TEM foil thickness using position averaged electron diffraction (inset in Fig. 1b to 1e) is essential for the analysis. While it has been suggested by DFT calculation that Al atomic prefers octahedral sites in an equilibrium growth condition, such as in bulk growth [4], the thin film growth typically occurs at non-equilibrium which leaves the preferred Al occupancy sites in question. Based on our analysis on β-(Al$_x$Ga$_{1-x}$)$_2$O$_3$ films with varying x (Fig. 1b to 1g), it has been revealed that the Al atoms indeed occupy both octahedral and tetrahedral sites, with an approximate ratio of (54:46), as shown in Fig. 1h. Therefore, we conclude that the Al occupancy at tetrahedral sites, which is metastable, can be attributed to the phase instability at Al concentration higher than 50%.

Formation of extended (planar) defects were also observed in these films (Fig. 2b), which provides important insights into the film growth mechanism. Our analysis revealed that the local atomic structure of the planar defect (Fig. 2b and 2c) resembles the structure of γ-phase Al$_2$O$_3$ (Fig. 2d and 2e). Furthermore, quantitative analysis of the column intensity revealed that the Al concentration becomes gradually lower at the closer vicinity to the planar defect, suggesting a correlation. The result leads to the conclusion that (*i*) the formation of the planar defect is due to the fluctuation in Al concentration during the growth, and (*ii*) the formation of the planar defect can therefore be the limiting factor for the epitaxy to continue beyond a certain critical film thickness. In summary, quantitative STEM provides atomic scale details of the structure of (Al$_x$Ga$_{1-x}$)$_2$O$_3$ that is essential to understand the growth and properties of the films, which are critical for the development of new oxide-based UWBG semiconductors for next-generation applications [5].
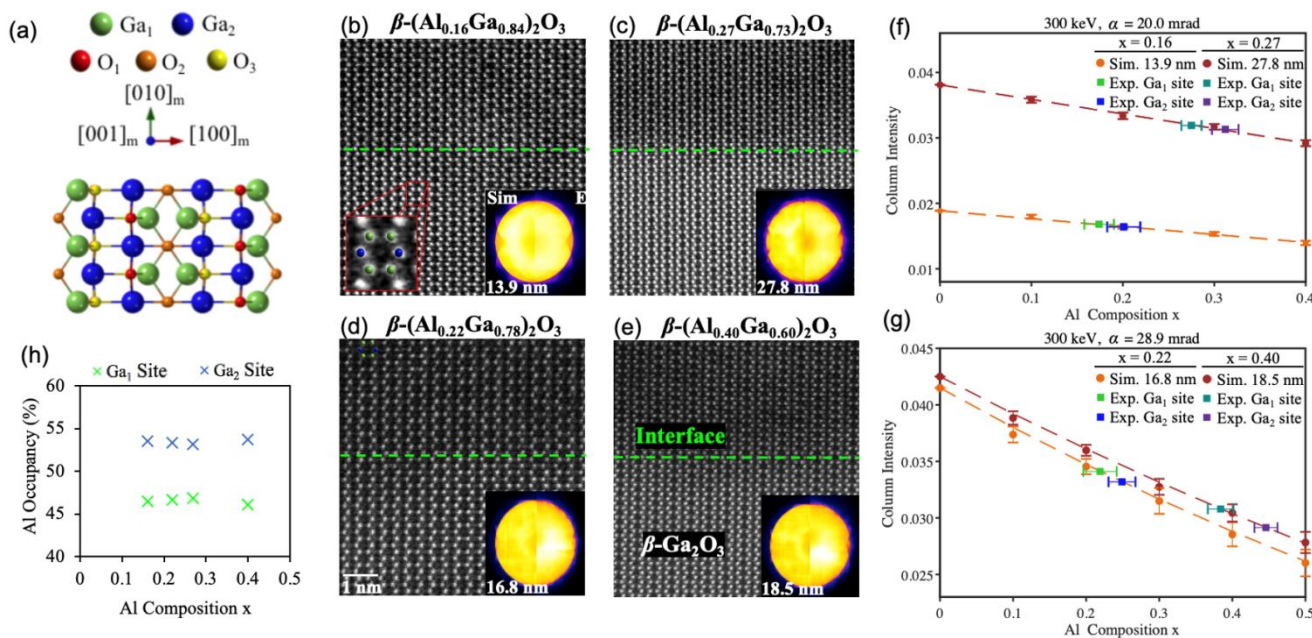
Figure 1. (a) Monoclinic Ga2O3. (b)-(e) HAADF images of (b) 16%, (c) 27%, (d) 22%, and (e) 40% of Al concentration in β-(AlxGa1-x)2O3. The inset shows thickness determined by PACBED: (b) 13.9 nm, (c) 27.8 nm, (d) 16.8 nm, and (e) 18.5 nm, respectively. (f) Quantitative HAADF intensity comparisons between the experimental data in (b) and (c) and multislice simulation results. (g) Quantitative HAADF intensity comparisons between the experimental data in (d) and (e) and multislice simulation results. (h) Plot displaying the Al site occupancy (%) in the Ga1 (green x) and Ga2 (blue x) sites versus the Al composition of the epifilms [3].
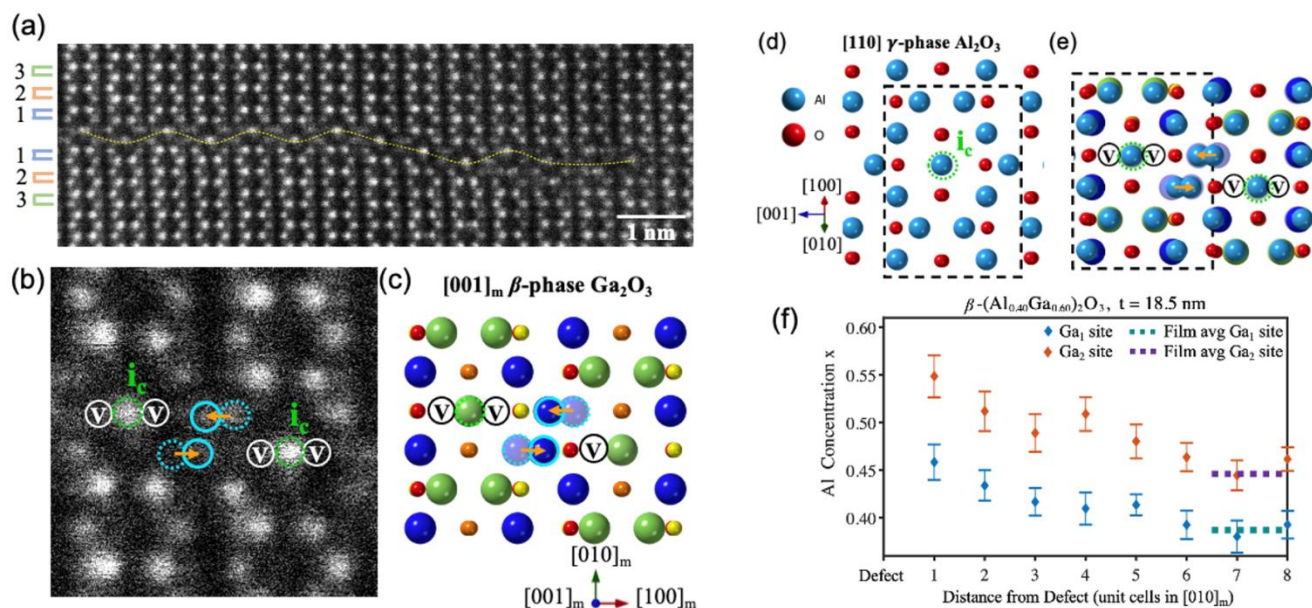

Figure 2. Figure 2: (a) Planar defects observed in β-(Al0.40Ga0.60)2O3 perpendicular to the (010) growth orientation. (b) A region of defect structure in (a), indicating the entirely vacant Ga1 site columns (V), adjacent ic site intensities (green dashed circle), and Ga2 intensities (blue circles) which have stabilized for the relaxed atomic structure. (c) Defect structure in β-phase configurations, the trajectory of relation (orange arrow), and

the final location (blue solid circle). (d) The gamma-phase of the Al2O3 structure, with the octahedrally coordinated atomic column located at the ic, is viewed along [110]. (e) Modeled [110] γ-Al2O3 indicates the defect structure resemblance visualized in (c). (f) Quantitative STEM characterization of Ga sites as a function of distance in unit cells (1-3 labeled in (a)), locating at the upper or lower defect structure interface. Experimental column intensities precisely compared to the β-(Al0.40Ga0.60)2O3 multislice simulation and the average film site occupations [3].

References
[1] M. H. Wong et al., IEEE Electron Device Lett. 37, 212 (2016).
[2] J. M. Johnson et al., Phys. Rev. X 9, 041027 (2019).
[3] J. M. Johnson et al., submitted.
[4] H. Peelaers et al., Appl. Phys. Lett. 112, 242101 (2018).
[5] This work was support by the Department of Defense, Air Force Office of Scientific Research GAME MURI Program (Grant No. FA9550-18-1-0479).